J Biomol NMR (2009) 45:207–216
DOI 10.1007/s10858-009-9344-9

ARTICLE

Chemical exchange effects during refocusing pulses in constant-time CPMG relaxation dispersion experiments

Wazo Myint · Rieko Ishima

Received: 15 May 2009 / Accepted: 22 June 2009 / Published online: 19 July 2009

Abstract In the analysis of the constant-time Carr-Purcell-Meiboom-Gill (CT-CPMG) relaxation dispersion experiment, chemical exchange parameters, such as rate of exchange and population of the exchanging species, are typically optimized using equations that predict experimental relaxation rates recorded as a function of effective field strength. In this process, the effect of chemical exchange during the CPMG pulses is typically assumed to be the same as during the free-precession. This approximation may introduce systematic errors into the analysis of data because the number of CPMG pulses is incremented during the constant-time relaxation period, and the total pulse duration therefore varies as a function of the effective field strength. In order to estimate the size of such errors, we simulate the time-dependence of magnetization during the entire constant time period, explicitly taking into account the effect of the CPMG pulses on the spin relaxation rate. We show that in general the difference in the relaxation dispersion profile calculated using a practical pulse width from that calculated using an extremely short pulse width is small, but under certain circumstances can exceed 1 s^{-1}. The difference increases significantly when CPMG pulses are miscalibrated.

Keywords Relaxation · CPMG · Off-resonance error · Dynamics · Protein · NMR

Electronic supplementary material The online version of this article (doi:10.1007/s10858-009-9344-9) contains supplementary material, which is available to authorized users.

W. Myint · R. Ishima (✉)
Department of Structural Biology, University of Pittsburgh School of Medicine, Rm 1037, Biomedical Science Tower 3, 3501 Fifth Avenue, Pittsburgh, PA 15260, USA
e-mail: ishima@pitt.edu

Introduction

Conformational exchange among two or more environments with distinct chemical shifts occurring on the milli-microsecond time scale can be detected based on the constant-time Carr-Purcell-Meiboom-Gill (CT-CPMG) relaxation dispersion experiment. This method has been applied to characterize biologically important processes such as protein folding and enzyme kinetics, which involve local conformational fluctuations (Loria et al. 1999; Tollinger et al. 2001; Wang et al. 2001; Mulder et al. 2002; Skrynnikov et al. 2002; Tolkatchev et al. 2003; Beach et al. 2005; Eisenmesser et al. 2005; Valentine and Palmer 2005; Brath et al. 2006; Korzhnev et al. 2006; Kovrigin et al. 2006; Labeikovsky et al. 2007; Sugase et al. 2007; Loria et al. 2008; Hass et al. 2009). In the CT-CPMG relaxation dispersion experiment, the nuclear spin transverse relaxation rate, R_2, is measured as a function of the effective field strength, ν_{CP}, that is related to the half-duration between CPMG pulses, τ_{CPMG}, according to $\tau_{CPMG} = 1/(4\nu_{CP})$. The total relaxation period (T_{CP}) for transverse relaxation is fixed while ν_{CP} is increased by the decreasing τ_{CPMG}. Chemical exchange parameters, such as the exchange rate, populations of the exchanging species, and difference in off-resonance frequencies between the exchanging species, are optimized by fitting the experimental R_2 dispersion profile using a two-site exchange or a multiple-site exchange equation.

The equation that is applied to optimize the parameters is either a numerical solution of Bloch-McConnell equation or its approximate analytical solution (McConnell 1958; Luz and Meiboom 1963; Carver and Richards 1972). In both approaches, the calculations typically neglect effects of chemical exchange during CPMG pulses (i.e., the calculations assume free precession, except for an instantaneous 180° rotation, during each CPMG pulse) (Fig. 1).

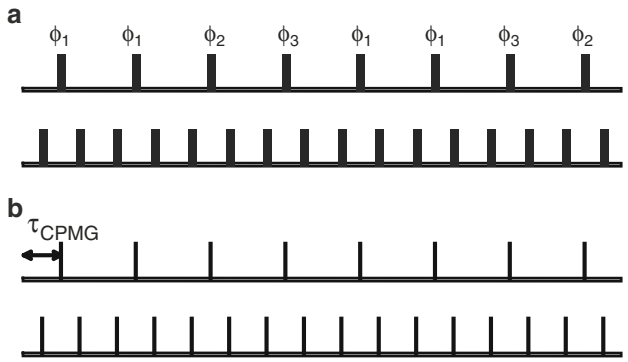

Fig. 1 Pulse schemes of the CT-CPMG relaxation experiments that are compared in this study: **a** includes pulse widths (*wide bars*) and **b** neglects pulse widths (*lines*). The CPMG pulse sequence utilizes the pulse phases $\phi_1 = \phi_2 = \phi_3 = X$ (Meiboom and Gill 1958) while an alternative sequence utilizes pulse phases of $\phi_1 = X$, $\phi_2 = Y$, $\phi_3 = -Y$ (Yip and Zuiderweg 2004; Long et al. 2008). In the following, these pulse schemes are denoted as the $[00000000]^{\pm}$ and the $[00130031]^{\pm}$ schemes, respectively. Entire phase cycles that were employed to calculate magnetization intensities in the following simulations are described in the Methods section

Although some studies take into account effects associated with off-resonance frequency (Ross et al. 1997; Ishima and Torchia 2003), the impact of neglecting the effect of the finite CPMG pulse duration on the calculated R_2 values is not known. Since the total duration of the CPMG pulses varies as a function of ν_{CP}, the total CPMG pulse duration ranges from as little as 0.45% up to 18% of the entire T_{CP} in typical ^{15}N CT-CPMG dispersion experiments (180° degree pulse, $\tau_{180} = 90$ μs; $\nu_{CP} = 25$–1000 Hz). Therefore, it is possible that the free-precession approximation during the pulse duration may introduce systematic error in the analysis of dispersion profiles.

The aim of this study is to determine whether the assumptions used in the analysis of ^{15}N CT-CPMG relaxation dispersion data with regards to the negligible width of pulses results in systematic error in the estimation of the chemical exchange parameters. For this purpose, the time-dependence of magnetization during the CT-CPMG period is calculated using the master equation for a two-state system, which accounts for chemical shift, radio-frequency pulse effects, relaxation, and chemical exchange (Allard et al. 1997, 1998; Myint et al. 2009). To determine the extent of systematic errors due to chemical exchange during CPMG pulses, the R_2 rates obtained with and without significant pulse widths, as illustrated in Fig. 1, are compared. Simulations are also performed using an alternative pulse scheme that was initially developed to reduce off-resonance effects on R_2 by Zuiderweg's group and subsequently applied for relaxation dispersion experiments by Yang's group (Yip and Zuiderweg 2004; Long et al. 2008), to determine whether systematic error exists in this alternative pulse sequence.

Methods

Master equation

The time evolution of bulk nuclear magnetization exchanging between two conformational sites, A and B, was calculated to determine the effect of pulse duration on the CT-CPMG relaxation dispersion experiment. The magnetization was represented by a state vector in which 7 Cartesian product operators were prepared as described previously (Allard et al. 1998)

$$\sigma(t) = \left[E/2 \quad M_X^A \quad M_Y^A \quad M_Z^A \quad M_X^B \quad M_Y^B \quad M_Z^B \right]^T \qquad (1)$$

with the $M_\gamma^{A/B}$ being the projection of the bulk magnetization vector of the site A or B along the $\gamma = X$, Y, or Z axis. The state vector is similar to the one used in the Bloch-McConnell equation (McConnell 1958) but includes a unity term E/2 that corresponds to the correction for equilibrium magnetization. The time evolution of $\sigma(t)$ through the pulse sequence was calculated by solving the master equation

$$\sigma(t + \Delta t) = \mathrm{Exp}(R \cdot \Delta t) \cdot \sigma(t) \qquad (2)$$

with the relaxation matrix, R, and an initial condition $\sigma(0)$ given by

$$R = -\begin{bmatrix} 0 & 0 & 0 & 0 & 0 & 0 & 0 \\ 0 & R_2^{0A} + k_{AB} & \Omega_A & \omega_Y^{B1} & -k_{BA} & 0 & 0 \\ 0 & -\Omega_A & R_2^{0A} + k_{AB} & -\omega_X^{B1} & 0 & -k_{BA} & 0 \\ -2R_1^{0A}M_{Z0}^A & -\omega_Y^{B1} & \omega_X^{B1} & R_1^{0A} + k_{AB} & 0 & 0 & -k_{BA} \\ 0 & -k_{AB} & 0 & 0 & R_2^{0B} + k_{BA} & \Omega_B & \omega_Y^{B1} \\ 0 & 0 & -k_{AB} & 0 & -\Omega_B & R_2^{0B} + k_{BA} & -\omega_X^{B1} \\ -2R_1^{0B}M_{Z0}^B & 0 & 0 & -k_{AB} & -\omega_Y^{B1} & \omega_X^{B1} & R_1^{0B} + k_{BA} \end{bmatrix} \qquad (3)$$

$$\sigma(0) = \begin{bmatrix} 1/2 & p_A & 0 & 0 & p_B & 0 & 0 \end{bmatrix}^T \quad (4)$$

R accounts for: the resonance frequencies of the two exchanging sites, Ω_A and Ω_B; the radio-frequency field, B_1, from the Y or X axis, ω_X^{B1} or ω_Y^{B1}; the intrinsic longitudinal relaxation rates for sites A and B, R_1^{A0} and R_1^{B0}, respectively; the intrinsic transverse relaxation rates for sites A and B, R_2^{A0} and R_2^{B0}, respectively; and the exchange rates from site A to site B, and from site B to site A, k_{AB} and k_{BA}, respectively. The $M_{Z0}^{A/B}$ is the equilibrium magnetization along the Z-axis for site A or B. The ω_X^{B1} and ω_Y^{B1} are related to the duration of an ideal 180° pulse width, τ_{180}, by the relation $\omega_{X/Y}^{B1} = \pi/\tau_{180}$. The fractional populations of sites A and B are given by p_A and p_B, respectively, with $p_A + p_B = 1$. The exchange rate, k_{ex}, is given by $k_{ex} = k_{AB}/p_B = k_{BA}/p_A$. The difference in chemical shifts, $(\delta\omega)/2\pi$, is defined by $(\Omega_A - \Omega_B)/2\pi$. The equation used here is different from the relaxation matrix that is often used for the optimization of chemical exchange parameters in CT-CPMG dispersion experiments in which longitudinal magnetization terms and effects of pulse duration are not taken into account (Korzhnev et al. 2004). Calculations were performed using the MATLAB software (The Mathworks Inc., Natick, MA).

Schemes for the CT-CPMG simulation

Simulations were conducted using the original CPMG pulse sequence in the following manner (denoted as a $[00000000]^{\pm}$ scheme). Transverse magnetization was generated initially along the X-axis as given by $\sigma(0)$, and the CPMG pulses were applied along the X-axis. Next, magnetization was again generated along the X-axis, and the CPMG pulses were applied along the $-X$-axis. The average of the magnetization intensities calculated these two ways at time T_{CP}, $M_X^i(T_{CP})$, was then used to calculate R_2 value according to

$$R_2^i = \ln\left(M_X^i(0)/M_X^i(T_{CP})\right)/T_{CP} \quad (5)$$

Here, i = A or B site. R_2 values for individual sites were calculated in the slow exchange case. The summation of A and B site magnetization was used for the calculation of R_2 in the fast exchange case. The superscript i to indicate site i is neglected to simplify the description hereafter. Superscript i in the intrinsic relaxation rates is also neglected hereafter by using conditions of $R_1^{A0} = R_1^{B0} = R_1^0$ and $R_2^{A0} = R_2^{B0} = R_2^0$. This condition will avoid additional systematic errors caused by differences in the intrinsic relaxation rates of the two sites (Ishima and Torchia 2006).

Simulations were also conducted using an alternative sequence that was proposed previously (Yip and Zuiderweg 2004; Long et al. 2008) (denoted as $[00130031]^{\pm}$). In this scheme, transverse magnetization was generated along the X-axis, and the 180° pulses were applied along the X, X, Y, $-Y$, X, X, $-Y$, Y axes with a minimum eight pulses in 1 cycle. Magnetization intensity after T_{CP} was stored in the memory. Next, magnetization was again generated in the X-axis, and the 180° pulses were applied from the $-X$, $-X$, $-Y$, Y, $-X$, $-X$, Y, $-Y$ axes with a minimum eight pulses in 1 cycle. Transverse magnetization at time T_{CP}, $M_X(T_{CP})$, was calculated as the average of the two magnetization intensities. Apparent relaxation rates for the $[00130031]^{\pm}$ scheme, R_{Alt}, were determined by Eq. (5), and corrected using Eq. (6) to yield R_2 values for R_2 dispersion plot (Long et al. 2008):

$$R_2 = R_{Alt} + \frac{(R_2^0 - R_1^0)\tau_{180}}{8\tau_{CPMG}} \quad (6)$$

When there is no chemical exchange (i.e., $R_2 = R_2^0$), the Eq. (6) is identical to that proposed by Zuiderweg for general transverse relaxation experiments (Yip and Zuiderweg 2004).

Parameters applied for CT-CPMG simulations

The following three sets of R_2 dispersion profiles were generated in this study using the $[00000000]^{\pm}$ and $[00130031]^{\pm}$ schemes described above. In all the simulations, R_1^0 and R_2^0 were set equal to 1.86 s^{-1} and 10.84 s^{-1}, respectively. This corresponds to amide nitrogens in a protein with a rotational correlation time of 7 ns at 60.8 MHz ^{15}N resonance frequency. Fractional populations, p_A and p_B, were set equal to 0.8 and 0.2, respectively. R_2 values were calculated for pulse sequences of $T_{CP} = 40$ ms and ν_{CP} ranging from 100 to 3,000 Hz, with R_2 values calculated for every $\nu_{CP} = 100$ Hz. Pulse width for CPMG was assumed to be either τ_{180} = 90 μs or 2 ns in all the simulations as described below.

The first set of R_2 dispersion profiles was calculated without any chemical exchange to determine the effects of off-resonance errors quantitatively. The simulations were conducted assuming accurate CPMG pulses that rotate on-resonance magnetization by 180°. The simulations were repeated assuming that the CPMG pulses were applied at a 20% lower B_1 field strength (that corresponds to 144° rotation of on-resonance magnetization). R_2 dispersion profiles were calculated for the resonances that are located at 0, 200, 400, and 800 Hz off-resonance from the carrier.

The second set of simulations was calculated allowing chemical exchange using the following parameters: (a) $k_{ex} = 5 \times 10^3$ s^{-1} and $\delta\omega/2\pi = 150$ Hz; (b) $k_{ex} = 20 \times 10^3$ s^{-1} and $\delta\omega/2\pi = 300$ Hz; (c) $k_{ex} = 100$ s^{-1} and $\delta\omega/2\pi = 500$ Hz; (d) $k_{ex} = 100$ s^{-1} and $\delta\omega/2\pi = 1{,}500$ Hz. Here, (a) and (b) satisfy the fast exchange condition ($k_{ex} \gg \delta\omega/2\pi$), and (c) and (d) satisfy the slow exchange

condition ($k_{ex} \ll \delta\omega/2\pi$). Accurate 180° pulses were assumed in the simulations, and site A was set at the on-resonance frequency.

The third set of simulations was calculated allowing chemical exchange assuming the CPMG pulses at 20% lower and 20% higher B_1 field strengths (corresponding to 144° and 216° rotations, respectively). In these simulations, following parameters were used: $k_{ex} = 20 \times 10^3$ s^{-1} and $\delta\omega/2\pi = 300$ Hz, and $k_{ex} = 100$ s^{-1} and $\delta\omega/2\pi =$ 1,500 Hz, which correspond to (b) and (d) in the above paragraph, respectively.

In the first and the second sets of simulations, R_2 dispersion profiles for the $[00000000]^{\pm}$ scheme were also calculated using an extremely short pulse width, $\tau_{180} = 2$ ns, to obtain an ideal CPMG R_2 profile. Additionally, $R_{1\rho}$ values were calculated as a function of the radio-frequency field, B_{SL} (=$\omega_{SL}/2\pi$), using the Palmer and Massi's equation (31) (Palmer and Massi 2006):

$$R_{1\rho} = R_1^0\cos^2\theta + R_2^0\sin^2\theta + \frac{p_A p_B \delta\omega^2 k_{ex}\omega_{SL}^2/\omega_e^2}{\omega_{eA}^2\omega_{eB}^2/\omega_e^2 + k_{ex}^2 - 2p_A p_B\delta\omega^2\gamma\omega_{SL}^2/\omega_e^2 + (1-\gamma)\omega_{SL}^2} \quad (7)$$

with $\gamma = 1 + p_A p_B \delta\omega^2\left(\frac{(p_A\Omega_B + p_B\Omega_A)^2 + \omega_{SL}^2 - k_{ex}^2}{\left((p_A\Omega_B + p_B\Omega_A)^2 + \omega_{SL}^2 + k_{ex}^2\right)^2}\right)$; $\bar{\Omega} = p_A\Omega_A + p_B\Omega_B$; $\theta = \arctan\left(\omega_{SL}/\bar{\Omega}\right)$; $\omega_e = \left(\bar{\Omega}^2 + \gamma\omega_{SL}^2\right)^{1/2}$; and $\omega_{ei} = \left(\Omega_i^2 + \gamma\omega_{SL}^2\right)^{1/2}$ (with i = A, B for effective field at site A or site B).

To evaluate differences of the calculated R_2 profiles from the ideal CPMG R_2 profile, the calculated R_2 profiles were fit by using the Bloch-McConnell equation with instantaneous 180° rotation (Fig. 1b). In the fitting, k_{ex} and p_A were optimized while R_2^0 and $\delta\omega/2\pi$ were fixed. The optimizations of the parameters were verified by grid searches to minimize ΔR_2 that was defined as r. m. s. d. between the calculated and the fit R_2 profiles. The uncertainties of the optimized parameters were given as the ranges in which $\Delta R_2 < 0.5$ s^{-1}. Since the simulations were conducted in the skewed population case (p_A:p_B = 0.8:0.2), the calculated R_2 profiles were plotted only for site A in slow exchange and for the weighted average magnetization in fast exchange.

Results and discussions

CPMG Simulations in the absence of chemical exchange

The aim of this study is to identify systematic error caused by the chemical exchange effects during pulses in the CT-CPMG R_2 dispersion experiments. Prior to conducting this research, we calculated time dependence of magnetization by solving Eq. (2) and determined R_2 based on Eq. (5) to quantitatively estimate off-resonance effects in the R_2 dispersion profile in the absence of chemical exchange (Ross et al. 1997). When the simulation was conducted by applying CPMG pulses at 5.56 kHz B_1 field strength (90 μs as 180° pulses), the observed R_2 values differed from the intrinsic relaxation rate, R_2^0, by up to 2, 4, and 7% at 200, 400, and 800 Hz off-resonance frequencies, respectively (Fig. 2a). However, these differences were still less than 1 s^{-1}. Off-resonance error was further reduced when the alternative CPMG experiment (Yip and Zuiderweg 2004; Long et al. 2008) ($[00130031]^{\pm}$ scheme) was applied. The maximum deviation of R_2 values from R_2^0 was less than 1% even at 800 Hz off-resonance frequency, providing uniform inversion over a significantly wider band width than the $[00000000]^{\pm}$ scheme (Fig. 2c).

We also simulated an extreme case when 144° pulses were applied instead of 180° rotation pulses for CPMG (20% miscalibration of the B_1 field strength). Although R_2 differed from R_2^0 by more than 5 s^{-1} at 800 Hz off-resonance frequency, the difference was less than 2 s^{-1} at <400 Hz off-resonance frequency (Fig. 2b). Such large difference of R_2 values from R_2^0 was not observed using the $[00130031]^{\pm}$ scheme, even when 144° pulse rotations were applied instead of 180° rotations (Fig. 2d). However, the calculated R_2 values were systematically ca. 1 s^{-1} smaller than R_2^0. This is because imperfect signal inversion pulse produces significant Z-magnetization that remains during the free-precession period between the pulses and results in contamination of R_1 component in the observed R_2 (see Supplementary material). Although the effect of R_1 during the pulses in $[00130031]^{\pm}$ scheme is taken into account in the calculation of R_2 values from R_{Alt} in Eq. (6), the effect of R_1 during free precession caused by the pulse imperfection remains.

Overall, the above simulations in the absence of chemical exchange demonstrate that the off-resonance error is less than 1 s^{-1} at <400 Hz off-resonance frequency when 180° pulse rotation is applied, and is less than 2 s^{-1} at <200 Hz off-resonance frequency even when 144° pulse rotation is applied. Thus, in the following simulations, we assumed a two-site exchange with site A at the carrier frequency in both slow and fast exchange cases. In the fast exchange simulation, $\delta\omega/2\pi$ was set to be either 150 or 300 Hz so that the weighted average resonance was located at 60 or 100 Hz, respectively. Such a narrow region was used to minimize off-resonance effect and to allow thereby the determination of systematic error caused by chemical exchange occurring during pulsing.

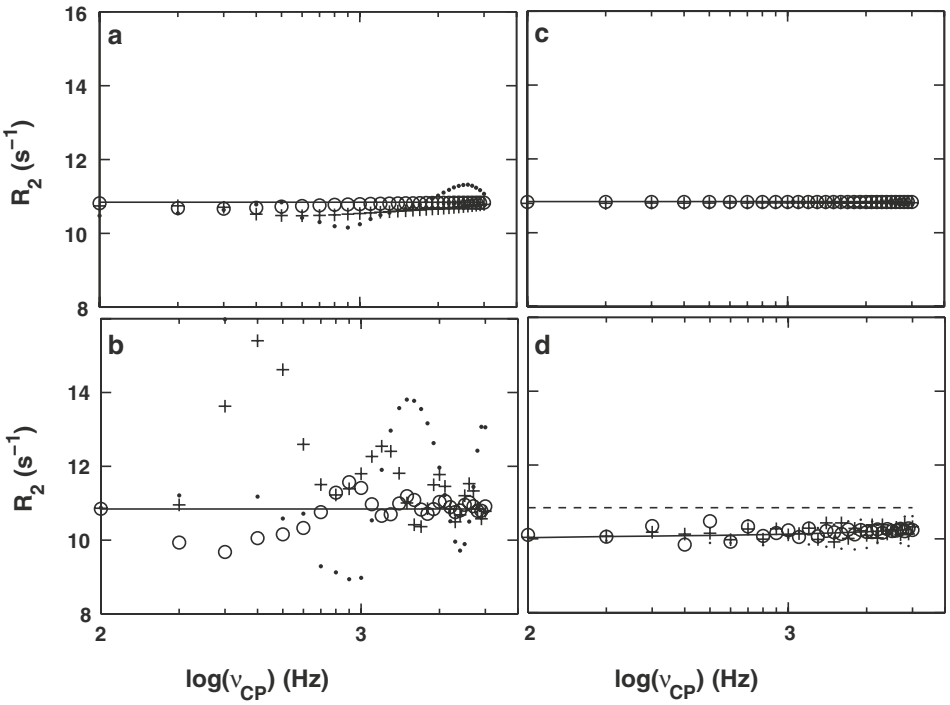

Fig. 2 R_2 values calculated as a function of effective field strength ν_{CP}, in the absence of chemical exchange for (**a**, **b**) $[00000000]^{\pm}$ and (**c**, **d**) $[00130031]^{\pm}$ schemes. Figures in (**a**) and (**c**) were calculated using ideal 180° rotation pulses, while Figures in (**b**) and (**d**) were calculated using 144° pulses instead of the 180° rotation pulses (assuming −20% B_1 miscalibration). In each figure, *solid line* (-), *circles* (○), *crosses* (+), and *dots* (•) indicate R_2 values calculated at 0, 200, 400, and 800 Hz from the radio-frequency carrier, respectively. In (**a**)–(**c**), the *solid lines* are consistent with the intrinsic transverse relaxation rate, R_2^0, used in the simulation. In (**d**), the *solid line* (i.e., R_2 at the carrier frequency) is significantly different from the R_2^0 that is shown by the *dashed line*. All the simulations were conducted using the following parameters: $\tau_{180} = 90$ μs, $R_1^0 = 1.86$ s^{-1}, and $R_2^0 = 10.84$ s^{-1}

Effects on pulse width in the $[00000000]^{\pm}$ scheme

Based on the above results associated with the off-resonance effects, we simulated CPMG R_2 dispersion profiles assuming a two-site exchange with sites A ($p_A = 0.8$, $\omega_A/2\pi = 0$ Hz) and B ($p_B = 0.2$, $\omega_B/2\pi = 150$ Hz) in the fast exchange condition, $k_{ex} = 5 \times 10^3$ s^{-1} and $\delta\omega/2\pi = 150$ Hz. To obtain R_2 dispersion profile, we generated time-dependent magnetization by solving Eq. (2), with the chemical exchange term given by Eq. (3). R_2 was calculated from the final magnetization intensities using Eq. (5) at each effective field. To identify effects of chemical exchange during pulsing, the simulation was conducted twice: first with a practical pulse width, $\tau_{180} = 90$ μs, and second with an extremely short pulse width for an ideal case, $\tau_{180} = 2$ ns. The R_2 dispersion profiles obtained by these simulations were almost identical to each other: the discrepancy in R_2 was ca. <0.5 s^{-1} even at $\nu_{CP} = 3$ kHz, indicating there is no systematic error caused by the pulse width (Fig. 3a).

Simulation of the R_2 dispersion profile was also conducted in another exchange condition in which k_{ex} is much larger than that described above, $k_{ex} = 20 \times 10^3$ s^{-1} and $\delta\omega/2\pi = 300$ Hz (Fig. 3b). Compared with Fig. 3a, the R_2 dispersion profile at larger k_{ex} (Fig. 3b) is shifted towards higher ν_{CP} values, with significant R_{ex} remaining at high ν_{CP} that is recorded after frequent CPMG pulses. In this case, R_2 calculated using $\tau_{180} = 90$ μs exhibited small but significant difference from the CPMG R_2 values calculated using $\tau_{90} = 2$ ns: discrepancy between the R_2 values at $\nu_{CP} = 1$ kHz was ca. 0.5 s^{-1}, and that at $\nu_{CP} = 3$ kHz was ca. 1.5 s^{-1} (6% reduction in R_2). Comparison of the R_2 dispersion profile with the relaxation rates calculated using a spin-lock demonstrate that the R_2 values calculated using $\tau_{180} = 90$ μs approach a spin lock profile at increasing ν_{CP} (Fig. 3b). This is because the fraction of the magnetization that remains along the X-axis under the applied radio-frequency field strength increases as ν_{CP} increases. When the R_2 profile simulated using $\tau_{180} = 90$ μs was fit using the Bloch-McConnell equation with instantaneous 180° rotation (and the fixed $R_2^0 = 10.84$ s^{-1} and $\delta\omega/2\pi = 300$ Hz), p_A and k_{ex} were optimized to be 0.765 ± 0.005 and $22.5 \pm 0.5 \times 10^3$ s^{-1}, respectively. These values correspond to changes of 0.035 and 2.5×10^3 s^{-1} from those originally used (0.80 and 20×10^3 s^{-1}) to generate the profile, respectively.

We next simulated CPMG R_2 dispersion profiles in slow exchange, $k_{ex} = 100$ s^{-1} and $\delta\omega/2\pi = 500$ Hz, assuming a two-site exchange with site A ($p_A = 0.8$, $\omega_A/2\pi = 0$ Hz)

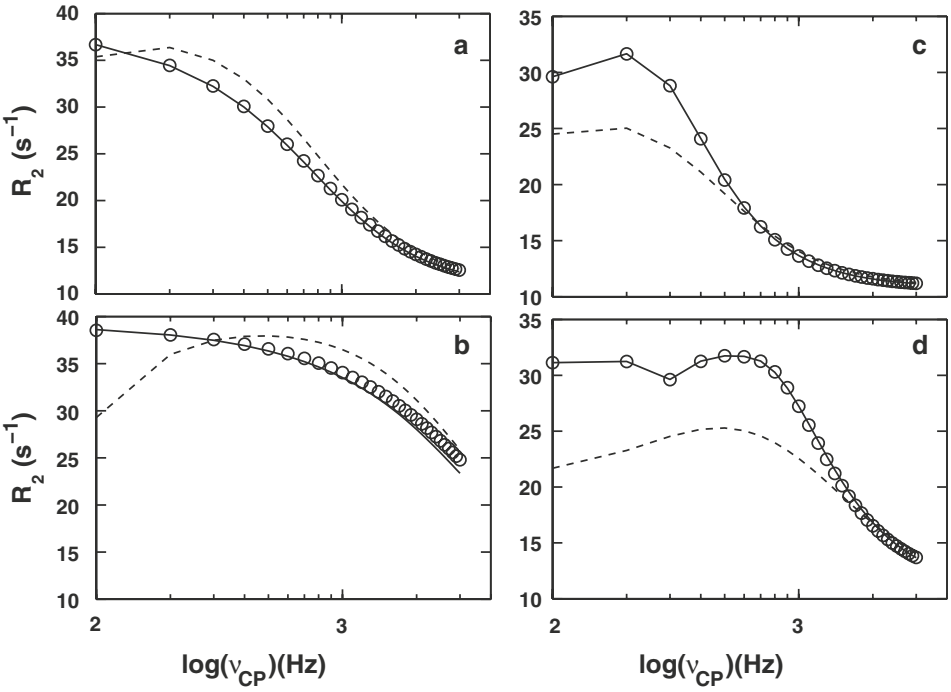

Fig. 3 R_2 dispersion profiles calculated in the presence of chemical exchange for (**a**, **b**) fast exchange and (**c**, **d**) slow exchange, using the $[00000000]^{\pm}$ scheme. In each figure, *circles* (○) and *line* (-) indicate R_2 profile calculated using a practical 180° pulse width ($\tau_{180} = 90$ μs) and the ideal CPMG R_2 profile calculated without significant pulse duration ($\tau_{180} = 2$ ns), respectively. Both of these profiles were generated assuming two-site exchange with $p_A = 0.8$, $p_B = 0.2$, $R_1^0 = 1.86\ s^{-1}$, and $R_2^0 = 10.84\ s^{-1}$, and with site A at the carrier frequency. Other parameters were: **a** $k_{ex} = 5 \times 10^3\ s^{-1}$ and $\delta\omega/2\pi = 150$ Hz; **b** $k_{ex} = 20 \times 10^3\ s^{-1}$ and $\delta\omega/2\pi = 300$ Hz; **c** $k_{ex} = 100\ s^{-1}$ and $\delta\omega/2\pi = 500$ Hz; **d** $k_{ex} = 100\ s^{-1}$ and $\delta\omega/2\pi = 1{,}500$ Hz. For comparison, relaxation rates in the rotating frame (spin-lock condition) were also plotted as a function of ν_{CP} (assuming $\nu_{CP} = B_{SL}$) by the *dashed line*

and B ($p_B = 0.2$, $\omega_B/2\pi = 500$ Hz). The R_2 dispersion profile simulated using $\tau_{180} = 90$ μs did not exhibit significant discrepancy from the ideal CPMG R_2 values (simulated using $\tau_{180} = 2$ ns) (Fig. 3c).

Even when the R_2 dispersion profile was calculated using a larger $\delta\omega/2\pi$ value, 1500 Hz, at $k_{ex} = 100\ s^{-1}$, no significant discrepancy was obtained (Fig. 3d). As described above, this is also because chemical exchange contribution in R_2 becomes small (<5 s^{-1}) at large ν_{CP} (>1 kHz). Since an increase in $\delta\omega/2\pi$ increases the R_2 values at large ν_{CP}, systematic errors caused by chemical exchange during the pulses may become significant when $\delta\omega/2\pi$ exceeds 1,500 Hz. However, such large $\delta\omega/2\pi$ values are expected to be rare in the spectra of diamagnetic proteins. Similarly, an R_2 dispersion profile calculated using a pulse width longer than $\tau_{180} = 90$ μs amplifies systematic error caused by the chemical exchange (see Supplementary material).

Effects on pulse width in the $[00130031]^{\pm}$ scheme

Using the same chemical exchange parameters as those applied to generate Fig. 3b ($k_{ex} = 20 \times 10^3\ s^{-1}$ and $\delta\omega/2\pi = 300$ Hz) and Fig. 3d ($k_{ex} = 100\ s^{-1}$ and $\delta\omega/2\pi = 1{,}500$ Hz), R_2 dispersion profiles were simulated using the $[00130031]^{\pm}$ scheme by solving Eq. (2) (Fig 4a, b, respectively). The apparent relaxation rate, R_{Alt}, was determined from the final magnetization intensities using Eq. (5), and finally R_2 value was calculated using Eq. (6) at each effective field.

R_2 dispersion profiles simulated using the $[00130031]^{\pm}$ scheme were almost the same as the ideal CPMG R_2 profiles calculated using the $[00000000]^{\pm}$ scheme with $\tau_{180} = 2$ ns (Fig. 4a, b). Especially, it is noteworthy that the dispersion profile calculated using the $[00130031]^{\pm}$ scheme does not approach the calculated $R_{1\rho}$ at increasing ν_{CP}. The agreement of the dispersion profile calculated using $\tau_{180} = 90$ μs to the ideal CPMG R_2 profiles calculated using the $\tau_{180} = 2$ ns can be explained by the assumptions used in the correction Eq. (6) for the $[00130031]^{\pm}$ scheme. By defining a duration for free precession as $2\tau_{FP} = 2\tau_{CPMG} - \tau_{180}$, the correction equation for the time average of R_{Alt} for the four echo periods of the [0013] phase cycle (X, X, Y, $-Y$) is recast as,

$$\begin{aligned} 8\tau_{CPMG}R_{Alt} &= 8\tau_{FP}R_2 + (3R_2 + R_1^0)\tau_{180} + 4(R_2 - R_2^0)\tau_{180} \\ &= 8\tau_{FP}R_2 + (3R_2^0 + R_1^0)\tau_{180} + 4R_{ex}\tau_{180} \end{aligned} \quad (8)$$

Here, $R_2 = R_2^0 + R_{ex}$. Equation (8) indicates that chemical exchange is described by a unique R_{ex} term

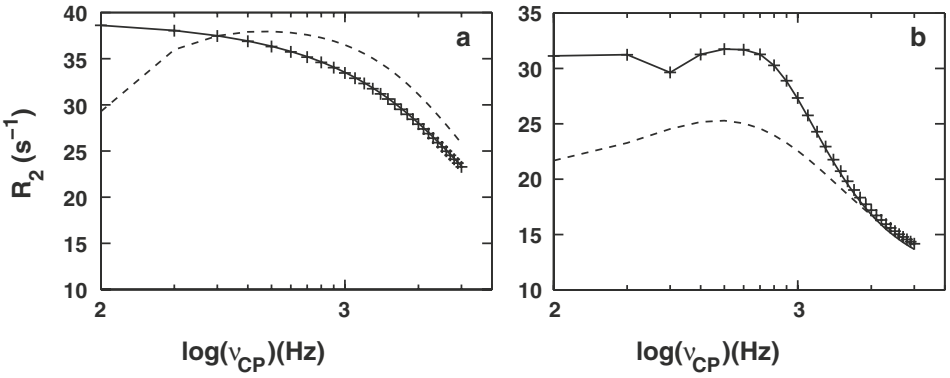

Fig. 4 R_2 dispersion profiles calculated in the presence of chemical exchange for **a** fast exchange and **b** slow exchange using the (+) $[00130031]^{\pm}$ scheme. The same values of the parameters used in Fig. 3b and d were employed to generate the profiles in figures (**a**) and (**b**), respectively. In each figure, *solid line* indicates the ideal CPMG R_2 profile calculated using the $[00000000]^{\pm}$ scheme with $\tau_{180} = 2$ ns, and the *dashed line* indicates relaxation rates in the rotating frame (spin-lock condition)

even during the pulse duration (the third term) as well as the free precession period. Thus, the dispersion profile is "reconstructed" using R_1^0, R_2^0, and R_{Alt} in Eq. (6) such that chemical exchange during pulsing is assumed to be the same as that in free-precession. Based on Eq. (8), the correction Eq. (6) is not sufficient to describe R_{Alt} that is calculated using a practical pulse width. However, significant error was not observed in R_2 calculated using the $[00130031]^{\pm}$ scheme in Fig. 4. This insignificance of the error is most likely due to cancellation of the increase in R_{ex} during X pulses by the decrease in R_{ex} during Y or $-Y$ pulses. In addition, when R_2 is used instead of R_2^0 in Eq. (6), resultant R_2 is overestimated. A question remains of how R_2^0 values can be measured accurately. Methods have been proposed to yield R_2^0 from the measurements of auto-relaxation rates (Ghose et al. 2001), cross-correlated relaxation values (Wang et al. 2001) or a combination of longitudinal, single, and double quantum coherence relaxation values (Hansen et al. 2007). However, these approaches require many additional measurements.

Effects on pulse width in the case of large pulse miscalibration

To estimate the magnitude of systematic errors that are introduced by miscalibration of the 180° pulse, R_2 dispersion profiles were also calculated using 144° and 216° pulses, representing −20% and +20% errors in the B_1 field strength. In the fast exchange (equivalent to that used in Fig. 3b, $k_{ex} = 20 \times 10^3$ s^{-1} and $\delta\omega/2\pi = 300$ Hz) using the $[00000000]^{\pm}$ scheme, R_2 dispersion profile generated for $\tau_{180} = 90$ μs at 20% lower B_1 field strength (shown by ○ in Fig. 5a) showed larger values than the ideal CPMG R_2 values (by the solid line in Fig. 5a assuming the correct 180° rotation and τ_{180}= 2 ns). This difference in R_2 values was more significant than that in Fig. 3b because of the 20% weaker B_1 field strength. When this R_2 profile (shown by ○ in Fig. 5a) was fit using the Bloch-McConnell equation with instantaneous 180° rotation (with the fixed $k_{ex} = 20 \times 10^3$ s^{-1} and $\delta\omega/2\pi = 300$ Hz), p_A and k_{ex} were optimized to be 0.635 ± 0.015 and $28.9 \pm 0.6 \times 10^3$ s^{-1}, respectively (corresponding to the 0.165 and 8.9 $\times 10^3$ s^{-1} differences from the values used to generate the profile, 0.8 and 20 $\times 10^3$ s^{-1}). At +20% higher B_1 field strength, the R_2 dispersion profile generated using the $[00000000]^{\pm}$ scheme (shown by ○ in Fig. 5b) was similar to that at −20% higher B_1 field strength but approached the spin-lock values of the +20% higher B_1 field strength.

In the slow exchange ($k_{ex} = 100$ s^{-1} and $\delta\omega/2\pi = 1{,}500$ Hz, which are equivalent to those in Fig. 3d) using the $[00000000]^{\pm}$ scheme, R_2 dispersion profiles generated for $\tau_{180} = 90$ μs at 20% lower or higher B_1 field strength (shown by ○ in Fig. 5c or d, respectively) were almost identical to the ideal CPMG R_2 profile calculated using the correct B_1 field strength for $\tau_{180} = 2$ ns. This is because the A site magnetization is located at on-resonance along the X-axis, and is not affected by the pulse effects. However, at higher ν_{CP} (>1 kHz), the R_2 profiles generated at 20% lower/higher B_1 field strength start to have discrepancy from the ideal CPMG R_2 profile and approach the spin-lock profile.

In contrast to the profiles calculated using the $[00000000]^{\pm}$ scheme, R_2 dispersion profiles calculated using the $[00130031]^{\pm}$ scheme for fast exchange at −20% and +20% errors in the B_1 field strength (described by + in Fig. 5a, b, respectively) mostly exhibited smaller R_2 values than those of the ideal CPMG R_2 profile calculated using the $[00000000]^{\pm}$ scheme at $\tau_{180} = 2$ ns (described by solid lines in Figs 5a, b). Discrepancy in R_2 value calculated using the $[00130031]^{\pm}$ scheme at 20% weaker/stronger B_1 field strength from that of the ideal CPMG R_2 profile was ca. 4 s^{-1} at $\nu_{CP} = 100$ Hz in Fig. 5a

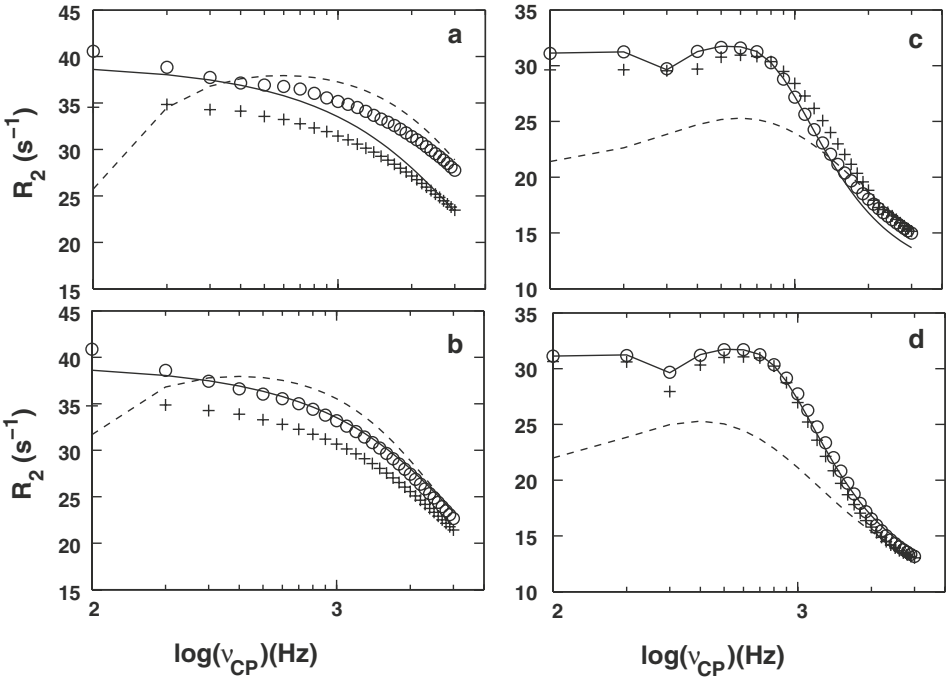

Fig. 5 R_2 dispersion profiles calculated for **a**, **b** fast exchange and **c**, **d** slow exchange by employing (**a**, **c**) 144° pulses (−20% B_1 miscalibration) or (**b**, **d**) 216° pulses (+20% B_1 miscalibration). In each figure, *circles* (○), and *crosses* (+) indicate R_2 values calculated using the $[00000000]^{\pm}$ and $[00130031]^{\pm}$ schemes, respectively. Other parameter values used for the simulations for the (**a**, **b**) fast exchange and (**c**, **d**) slow exchange were the same as those employed to generate the profiles in Fig. 3b and d, respectively. In each figure, an ideal CPMG R_2 profile calculated with extremely short pulse duration using the $[00000000]^{\pm}$ scheme is shown by the *solid line*, and the profile calculated using the spin-lock condition at (**a**, **c**) −20% lower or (**b**, **d**) +20% higher B_1 field strength is shown by the *dashed line*

and b, and was significantly larger than that observed in the absence of chemical exchange in Fig. 2d. This is because Eq. (6) does not include the effects of the residual Z-magnetization during the free-precession period (as shown in the Supplementary material). When the R_2 profile calculated with 20% weaker B_1 field in (indicated by + in Fig. 5a) was fit using the Bloch-McConnell equation for the $[00000000]^{\pm}$ scheme with instantaneous 180° rotation at a correct B_1 field strength (and the fixed $k_{ex} = 20 \times 10^3$ s^{-1} and $\delta\omega/2\pi = 300$ Hz), p_A and k_{ex} were optimized to be 0.794 ± 0.007 and $23.4 \pm 0.8 \times 10^3$ s^{-1} (0.006 and 3.4×10^3 s^{-1} changes from those originally used to generate the profiles, 0.80 and 20×10^3 s^{-1}, respectively).

R_2 dispersion profiles were calculated for slow exchange assuming −20 and +20% errors in the B_1 field strength using the $[00130031]^{\pm}$ scheme (described by + in Fig. 5c, d, respectively). Other simulation conditions for these were the same as those applied to calculate the profiles shown in Fig. 3d. In both −20 and +20% B_1 error cases, most of the R_2 profiles were slightly smaller that the ideal CPMG R_2 profile calculated using the correct B_1 field strength for $\tau_{180} = 2$ ns. (described by the solid line in Fig. 5c, d). The discrepancy was almost equivalent to that observed in the profile calculated without chemical exchange in Fig. 2d. At high $\nu_{CP} > 1$ kHz, the R_2 values approaches the spin-lock profile (Fig. 5c). For these slow exchange profiles calculated using miscalibrated pulses, optimized parameters using the Bloch-McConnell equation with instantaneous 180° rotation are not shown because they were not fit satisfactorily ($\Delta R_2 > 0.5$ s^{-1}).

Summary

In this study, we have compared effect of chemical exchange contribution during pulsing in the CT-CPMG experiments by computer simulation. Exchanging signals were located close to the radio-frequency carrier in order to estimate the errors that arise by chemical exchange during the CPMG pulses, without introducing errors from the off-resonance effects. R_2 profiles that were simulated in different conditions from those described above, such as the case that signal is not close to the carrier frequency, are shown in the Supplementary material.

R_2 dispersion profile that was calculated using the standard CPMG $[00000000]^{\pm}$ scheme with a practical pulse width was shown to approach spin-lock equation in fast exchange, particularly when k_{ex} is large ($>10 \times 10^3$ s^{-1}). Although this error in the R_2 profile is

small ($\sim 1\ s^{-1}$, Fig. 3b), such error that is caused by chemical exchange during pulsing is systematically associated with the effective field strength. Consequently, when the pulse duration effect is not taken into account in the fitting of the data, this systematic error shifts the optimized exchange parameters from those originally used to generate the profile (for example, changes in p_A and k_{ex} were 3.5 and 12.5%, respectively, in Fig. 3b). To avoid misinterpretation of the exchange parameters, it will be necessary to collect dispersion data of other nuclei, such as ^1H, that can be recorded using a short pulse width. When an alternative pulse scheme, $[00130031]^{\pm}$ (Yip and Zuiderweg 2004; Long et al. 2008), was employed, chemical exchange during pulsing did not introduce significant systematic errors in the R_2 profiles. Nevertheless, when the inversion pulse is miscalibrated, R_2 values calculated using the $[00130031]^{\pm}$ scheme with a practical pulse width is systematically reduced because of significant R_1 relaxation effects during the free-precession period.

Acknowledgments We thank Eva Meirovitch, Daiwen Yang, and Dennis Torchia for useful discussions and/or critical reading of the manuscript. This study was financially supported by the American Heart Association (Great Rivers affiliate) new investigator grant 0765348U, and National Science Foundation research grant MCB 0814905. Supplementary material is available.

References

Allard P, Helgstrand M, Hard T (1997) A method for simulation of NOESY, ROESY, and Off-resonance ROESY spectra. J Magn Reson 129:19–29

Allard P, Helgstrand M, Hard T (1998) The complete homogeneous master equation for a heteronuclear two-spin system in the basis of Cartesian product operators. J Magn Reson 134:7–16

Beach H, Cole R, Gill ML, Loria JP (2005) Conservation of mu s-ms enzyme motions in the apo- and substrate-mimicked state. J Am Chem Soc 127:9167–9176

Brath U, Akke M, Yang D, Kay LE, Mulder FA (2006) Functional dynamics of human FKBP12 revealed by methyl 13C rotating frame relaxation dispersion NMR spectroscopy. J Am Chem Soc 128:5718–5727

Carver JP, Richards RE (1972) General 2-site solution for chemical exchange produced dependence of T2 upon Carr-Purcell pulse separation. J Magn Reson 6:89–105

Eisenmesser E, Millet O, Labeikovsky W, Korzhnev D, Wolf-Watz M, Bosco DA, Skalicky JJ, Kay LE, Kern D (2005) Intrinsic dynamics of an enzyme underlies catalysis. Nature 438:117–121

Ghose R, Fushman D, Cowburn D (2001) Determination of the rotational diffusion tensor of macromolecules in solution from nmr relaxation data with a combination of exact and approximate methods—application to the determination of interdomain orientation in multidomain proteins. J Magn Reson 149:204–217

Hansen DF, Yang D, Feng H, Zhou Z, Wiesner S, Bai Y, Kay LE (2007) An exchange-free measure of 15N transverse relaxation: an NMR spectroscopy application to the study of a folding intermediate with pervasive chemical exchange. J Am Chem Soc 129:11468–11478

Hass MA, Vlasie MD, Ubbink M, Led JJ (2009) Conformational exchange in pseudoazurin: different kinds of microsecond to millisecond dynamics characterized by their pH and buffer dependence using 15N NMR relaxation. Biochemistry 48:50–58

Ishima R, Torchia DA (2003) Extending the range of amide proton relaxation dispersion experiments in proteins using a constant-time relaxation-compensated CPMG approach. J Biomol NMR 25:243–248

Ishima R, Torchia DA (2006) Accuracy of optimized chemical-exchange parameters derived by fitting CPMG R2 dispersion profiles when R2(0a) not = R2(0b). J Biomol NMR 34:209–219

Korzhnev DM, Kloiber K, Kay LE (2004) Multiple-quantum relaxation dispersion NMR spectroscopy probing. J Am Chem Soc 126:7320–7329

Korzhnev DM, Neudecker P, Zarrine-Afsar A, Davidson AR, Kay LE (2006) Abp1p and Fyn SH3 domains fold through similar low-populated intermediate states. Biochemistry 45:10175–10183

Kovrigin EL, Kempf JG, Grey MJ, Loria JP (2006) Faithful estimation of dynamics parameters from CPMG relaxation dispersion measurements. J Magn Reson 180:83–104

Labeikovsky W, Eisenmesser EZ, Bosco DA, Kern D (2007) Structure and dynamics of pin1 during catalysis by NMR. J Mol Biol 367:1370–1381

Long D, Liu M, Yang D (2008) Accurately probing slow motions on millisecond timescales with a robust NMR relaxation experiment. J Am Chem Soc 130:2432–2433

Loria JP, Rance M, Palmer AG (1999) A relaxation-compensated Carr-Purcell-Meiboom-Gill sequence for characterizing chemical exchange by NMR spectroscopy. J Am Chem Soc 121:2331–2332

Loria JP, Berlow RB, Watt ED (2008) Characterization of enzyme motions by solution NMR relaxation dispersion. Acc Chem Res 41:212–221

Luz Z, Meiboom S (1963) Nuclear magnetic resonance study of the protolysis of trimethylammonium ion in aqueous solution—order of the reaction with respect to solvent. J Chem Phys 39:366–370

McConnell HM (1958) Reaction rates by nuclear magnetic resonance. J Chem Phys 28:430–431

Meiboom S, Gill D (1958) Modified spin-echo method for measuring nuclear relaxation times. Rev Sci Instrm 29:688–691

Mulder FA, Hon B, Mittermaier A, Dahlquist FW, Kay LE (2002) Slow internal dynamics in proteins: application of NMR relaxation dispersion spectroscopy to methyl groups in a cavity mutant of T4 lysozyme. J Am Chem Soc 124:1443–1451

Myint W, Gong Q, Ishima R (2009) Practical aspects of 15N CPMG transverse relaxation experiments for proteins in solution. Concepts Magn Reson 34A:63–75

Palmer AG 3rd, Massi F (2006) Characterization of the dynamics of biomacromolecules using rotating-frame spin relaxation NMR spectroscopy. Chem Rev 106:1700–1719

Ross A, Czisch M, King GC (1997) Systematic errors associated with the CPMG pulse sequence and their effect on motional analysis of biomolecules. J Magn Reson 124:355–365

Skrynnikov NR, Dahlquist FW, Kay LE (2002) Reconstructing NMR spectra of "invisible" excited protein states using. J Am Chem Soc 124:12352–12360

Sugase K, Dyson HJ, Wright PE (2007) Mechanism of coupled folding and binding of an intrinsically disordered protein. Nature 447:1021–1025

Tolkatchev D, Xu P, Ni F (2003) Probing the kinetic landscape of transient peptide-protein interactions by use of peptide (15)n NMR relaxation dispersion spectroscopy: binding of an anti-thrombin peptide to human prothrombin. J Am Chem Soc 125:12432–12442

Tollinger M, Skrynnikov NR, Mulder FA, Forman-Kay JD, Kay LE (2001) Slow dynamics in folded and unfolded states of an SH3 domain. J Am Chem Soc 123:11341–11352

Valentine ER, Palmer AG 3rd (2005) Microsecond-to-millisecond conformational dynamics demarcate the GluR2. Biochemistry 44:3410–3417

Wang C, Grey MJ, Palmer AG 3rd (2001) CPMG sequences with enhanced sensitivity to chemical exchange. J Biomol NMR 21:361–366

Yip GN, Zuiderweg ER (2004) A phase cycle scheme that significantly suppresses offset-dependent artifacts in the R2-CPMG 15N relaxation experiment. J Magn Reson 171:25–36